Aalborg Universitet

AALBORG UNIVERSITY

Analysis of Impacts of Expected RF EMF Exposure Restrictions on Peak EIRP of 5G User Equipment at 28 GHz and 39 GHz Bands

Xu, B.; Zhao, Kun; Ying, Z.; Sjöberg, D.; He, W.; He, S.

Analysis of Impacts of Expected RF EMF Exposure Restrictions on Peak EIRP of 5G User Equipment at 28 GHz and 39 GHz Bands

BO XU[1,2,3], (Member, IEEE), **KUN ZHAO**[4,5], **ZHINONG YING**[4], (Senior Member, IEEE),
DANIEL SJÖBERG[6], (Senior Member, IEEE), **WANG HE**[1], AND **SAILING HE**[1,2], (Fellow, IEEE)

[1]Centre for Optical and Electromagnetic Research, Zhejiang University, Hangzhou 310058, China
[2]Department of Electromagnetic Engineering, KTH Royal Institute of Technology, SE-100 44 Stockholm, Sweden
[3]Ericsson Research, Ericsson AB, SE-164 80 Stockholm, Sweden
[4]Network Technology Lab, Research and Technology, Sony Mobile Communications AB, SE-221 88 Lund, Sweden
[5]Department of Electronic Systems, Antennas, Propagation and Radio Networking Section, Aalborg University, 9220 Alborg, Denmark
[6]Department of Electrical and Information Technology, Lund University, SE-221 00 Lund, Sweden

Corresponding author: Sailing He (sailing@jorcep.org)

ABSTRACT Above 6 GHz, radio frequency (RF) electromagnetic field (EMF) exposure from the mobile communication user equipment (UE) should be assessed in terms of incident power density, rather than specific absorption rate as below 6 GHz. Such regulatory RF EMF restrictions will constrain the transmit power of the UE and its peak equivalent isotropically radiated power (EIRP). This paper provides an analysis of the peak EIRP levels of UE containing code-book-based beamforming arrays at 28 GHz and 39 GHz. Different types of antenna elements, incremental element spacing, 4- and 8-element array configurations, and realistic housing integration are considered. The analysis and results show that in realistic housing integration, the 3GPP requirements on minimum peak EIRP can be generally met under the expected RF EMF exposure restrictions.

INDEX TERMS 5G, antenna array, EIRP, RF EMF exposure, incident power density, millimeter wave, user equipment.

I. INTRODUCTION

The first 3rd Generation Partnership Project (3GPP) release of the fifth-generation mobile communication (5G) New Radio (NR) specifications was delivered in June 2018. One key feature of NR is the deployment of much higher frequency bands above 24 GHz [1], [2] supporting very wide bandwidths to enable larger data volumes. The 28 GHz region and the 39 GHz region[1] are considered for the first 5G millimeter-wave (mmWave) commercial user equipment (UE) products. In these frequency bands, antenna dimensions are compact, so that beamforming antenna arrays can be integrated into UEs, such as mobile phones, tablets, and laptops, to compensate for higher free space path loss and extend coverage [3], [4]. In addition, the coexistence

The associate editor coordinating the review of this manuscript and approving it for publication was Jordi Mongay Batalla.

[1]including 3GPP NR bands n257 (26.5–29.5 GHz), n258 (24.25–27.5 GHz), n260 (37–40 GHz), and n261 (27.5–28.35 GHz) [2].

of 2G–5G technologies in one device determines that the 5G mmWave radio frequency (RF) modules would also coexist with 2G–4G RF modules. Due to the limited space in UE and the costly mmWave components, the 5G mmWave UE, at least for the initial realizations, would not contain a large amount of antenna elements. Therefore, 4-element [4], [5] or 8-element antenna arrays [6]–[9] using code-book-based beamforming would be expected to be the initial solutions for mmWave UE.

A UE transmitting wireless signals needs to comply with relevant safety guidelines constraining human exposure to RF electromagnetic fields (EMFs). The RF EMF exposure limits specified in terms of specific absorption rate (SAR), power density, or other metrics prevent, with great safety margins, from established adverse health effects associated with excessive localized tissue heating and whole-body heat stress. International RF EMF exposure guidelines have been published by the International Commission on Non-Ionizing

Radiation Protection (ICNIRP) [12] and the IEEE [14], [15]. The U.S. Federal Communication Commission (FCC) also specifies RF EMF exposure limits [10]. However, the current RF EMF exposure limits were published or updated years ago (ICNIRP in 1998, IEEE in 2010, and FCC in 1996), and are now undergoing revision. In July 2018, the ICNIRP published a draft of the new guidelines for public consultation [13]. Later in October, the IEEE International Committee on Electromagnetic Safety (ICES) released the latest draft of the revised C95.1 standard [16]. The draft IEEE and ICNIRP guidelines with updated RF EMF exposure limits are expected to be officially published in 2019. In 2015, the FCC proposed a change regarding RF EMF exposure limits above 6 GHz [17], and in October 2018, it proposed further changes in the near future at the Telecommunication Certification Body (TCB) workshop [11].

As a consequence of restricting RF EMF exposure, the transmit power of UE cannot exceed a certain level, which relates to mobile antenna design, and further the uplink equivalent isotropically radiated power (EIRP) is constrained [18]–[23]. On the other hand, the 3GPP specifies requirements on the range of EIRP and total radiated power (TRP) for UE to ensure enough link budget and also limit interference [2], as shown in Table 1. This naturally raises the question of whether the 3GPP requirements could be met considering the need to comply with applicable RF EMF exposure limits and regulations. A previous work [20] provided general information on current RF EMF regulations and on their possible implications on power limits for 5G NR handheld devices. Based on the latest available information, this paper investigates 4×1 and 8×1 array configurations at 28 GHz and 39 GHz considering a realistic housing integration.

TABLE 1. 3GPP NR specifications on EIRP and TRP for power class 3 UE (unit: dBm) [2].

f (GHz)	Peak EIRP	EIRP at 50th percentile CDF	Max TRP
24.25–29.5	≥ 22.4	≥ 11.5	≤ 23
37–40	≥ 20.6	≥ 8	≤ 23

The paper is organized as follows. Section II presents the current and proposed RF EMF exposure limits above 6 GHz in terms of incident power density. In Section III, the impacts of the expected RF EMF exposure restrictions on EIRP of different 28 GHz UE mock-ups are analyzed using various types of antenna elements, different element spacing, and different numbers of antenna elements. With a similar procedure, the impacts of the expected RF EMF exposure restrictions on EIRP of 39 GHz UE mock-ups and difference between the 28 GHz results and the 39 GHz results are presented in Section IV. Section V and VI are discussion and conclusion, respectively.

II. RF EMF EXPOSURE LIMITS ABOVE 6 GHz

As mentioned above, the RF EMF exposure limits protect against established adverse health effects in humans associated with exposure to electric, magnetic and electromagnetic fields. Below a transition frequency (6 GHz for the proposed guidelines), the compliance of UE usually needs to be determined using SAR evaluations. Above the transition frequency, the penetration depth of the EMFs into tissues is smaller as the frequency increases, and the correlation between SAR and the rising temperature is not as strong as at lower frequencies. In the draft ICNIRP guidelines, the transmitted power density (classified as basic restriction) and the incident power density (classified as reference level) are the metrics for local exposure above 6 GHz. In the draft IEEE guidelines, the epithelial power density (classified as dosimetric reference limit) and the incident power density (classified as exposure reference level) are the metrics for local exposure above 6 GHz. The metric for the proposed FCC limits is incident power density. The detailed description of the rationale for the chosen RF EMF exposure metrics and limits can be found in the ICNIRP public consultation document [13], its Appendices [24], [25], and the draft IEEE standard [16]. However, the epithelial power density and the transmitted power density are much more challenging and complicated for both calculation and measurement compared to the incident power density. The incident power density is considered as the more realistic metric for compliance tests. A brief summary and comparison of the current and proposed incident power density limits are listed in Table 2. One thing to notice is that the transition frequency is harmonized to 6 GHz by the ICNIRP, IEEE, and FCC, while the current limits have different transition frequencies. Another thing to notice is that unlike the current FCC and IEEE limits, all the proposed limits only require spatial-average incident power density, though the values of the limits and the sizes of averaging area are not harmonized. The FCC proposed to average incident power density over $1 \, \text{cm}^2$ in 2015 [17], while very recently at the 2018 TCB workshop, the FCC informed that the size of the averaging area will be changed to $4 \, \text{cm}^2$ for local exposure [11].

Assume the UE employs a code book of array excitations $\{\boldsymbol{w}_1, \boldsymbol{w}_2, \ldots, \boldsymbol{w}_{N_b}\}$ that can generate N_b number of beams. The code-book-based beamforming strategy is very likely to be implemented in 5G UE, at least in the beginning of 5G deployment, as it is less expensive and less complicated compared to reciprocity-based beamforming.[2] As shown in Fig. 1, at a perpendicular separation distance d above UE, the maximum spatial-average incident power density for the ith excitation $\boldsymbol{w}_i$ by sweeping the averaging area A over the plane is

$$S(d, \boldsymbol{w}_i) = \max_{\text{all areas}} \frac{1}{2A} \iint_A \text{Re} \left[\boldsymbol{E}(d, \boldsymbol{w}_i) \times \boldsymbol{H}^*(d, \boldsymbol{w}_i) \right] \cdot \hat{\boldsymbol{n}} \, dA, \quad (1)$$

where $\hat{\boldsymbol{n}}$ denotes the unit vector normal to the UE surface.

---

[2] The upper bound of incident power density for antenna arrays using reciprocity-based beamforming can be derived using the field-combining method and semidefinite relaxation [26].

TABLE 2. RF EMF exposure limits for general public in incident power density [10]–[16].

		Current			Proposed	
	f (GHz)	spatial-peak/averaging area	S_{lim} (W/m²)	f (GHz)	averaging area	S_{lim} (W/m²)
ICNIRP	10–300	1 cm²	200	6–30	4 cm²	$55f^{-0.177}$
		20 cm²	10	30–300	1 cm²	
IEEE	3–30ᵃ	spatial peak	$18.56f^{0.699}$			
		100λ^2	10			
	30–100	spatial peak	200	6–300ᵇ	4 cm²	$55f^{-0.177}$
		100 cm²	10			
	100–300	spatial peak	200			
		100 cm²	$(90f - 7000)/200$			
FCC	6–100	spatial peak	10	6–100	4 cm²	10

Notes:
When calculating S_{lim}, f is the frequency in GHz. For example, at 28 GHz, $55f^{-0.177} = 55 \times 28^{-0.177} \approx 30.5 \text{ W/m}^2$, and at 39 GHz, $55f^{-0.177} = 55 \times 39^{-0.177} \approx 28.8 \text{ W/m}^2$.
ᵃ Between 3 GHz–6 GHz, compliance can be evaluated by either incident power density or SAR.
ᵇ Small exposed areas above 30 GHz: If the exposed area on body surface is small ($< 1 \text{ cm}^2$ as defined by -3 dB contours relative to the peak exposure), the incident power density is allowed to exceed $55f^{-0.177}$ by a factor of 2, with an averaging area of 1 cm².
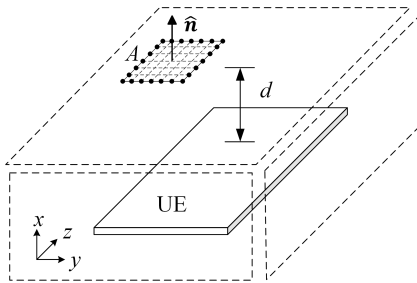
FIGURE 1. Sampling scheme of averaging areas in the Cartesian coordinate system with a separation distance *d*. Power densities in ±*x*, ±*y*, and ±*z*-directions are considered.

Considering all the beams, the maximum incident power density can be written as

$$S_{\text{max}}(d) = \max_{i=1,2,\ldots,N_b} S(d, \mathbf{w}_i). \tag{2}$$

Although the RF EMF exposure guidelines stipulate that incident power density should be averaged over a certain time and UE would not transmit with a fixed beam in practice, stating compliance may only be subjected to the theoretical maximum case, which is considered in this paper.

## III. RF EMF EXPOSURE RELATED RESTRICTION ON PEAK EIRP AT 28 GHz

A. SIMULATION SETTINGS

In the mmWave frequency range, the full-wave simulation of the entire UE is very time-consuming. To facilitate the RF EMF exposure study, three simplified UE mock-ups operating at 28 GHz and equipped with 4 × 1 arrays containing patch elements, notch elements [4], and slot elements, respectively, were used. The simulation models of these are shown in Fig. 2 operating at 28 GHz, and the geometric dimensions are shown in Fig. 3. The antennas are printed on a Rogers RO4003 substrate (29 mm × 14 mm × 0.3 mm, $\epsilon_r = 3.55$) with element spacing of $D = 5$ mm ($0.47\lambda_0$, λ_0
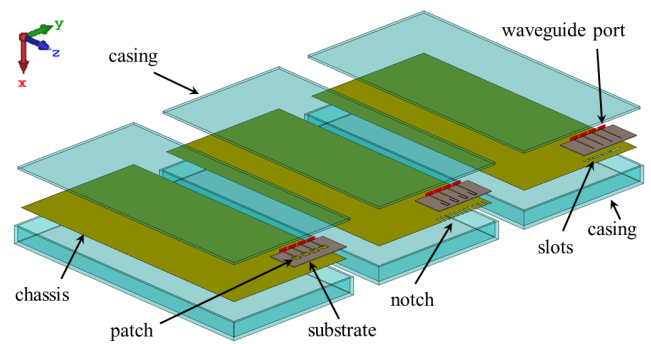
FIGURE 2. Exploded view of simulation models of 28 GHz UE mock-ups containing 4 × 1 patch array (left), notch array (middle), and slot array (right). Element spacing *D* = 5 mm.
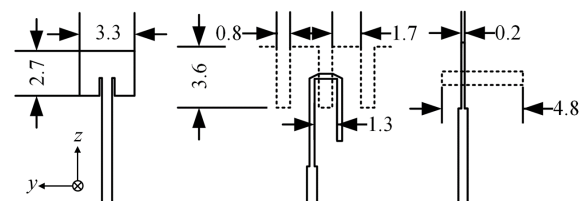
FIGURE 3. Geometry and dimensions of 28 GHz antenna elements (unit: mm).

is the free space wavelength). The substrate is mounted on the corner of the 126 mm × 62 mm chassis, and a plastic box (130 mm × 66 mm × 8 mm, $\epsilon_r = 3$) with thickness 1 mm is used to simulate the UE casing. The distance between the antennas and the UE casing is less than 2 mm. Patch, notch, and slot antennas are three typical antenna designs for UE with complementary radiation patterns and polarization in order to provide a good basis for comparison.

The code book of the array excitations is chosen based on the progressive phase shift scheme $\mathbf{w}_i = [a, ae^{-j\beta_i}, ae^{-j2\beta_i}, \ldots, ae^{-j(N_e-1)\beta_i}]$, in which a is the amplitude of excitation, β_i is the phase shift angle between adjacent
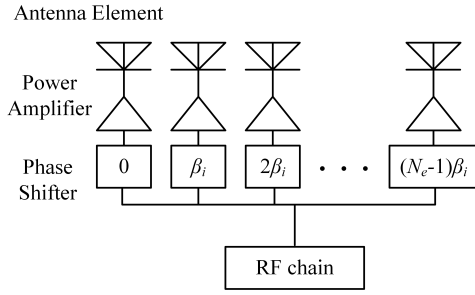
FIGURE 4. Phase excitation scheme with progressive phase shift β_i for N_e number of antenna elements.

FIGURE 5. Scan patterns of the 28 GHz mock-up containing 4 × 1 patch array when the progressive phase shift angle β_i increases from $-5\pi/6$ to $5\pi/6$ by a step of $\pi/6$ ($D = 5$ mm). The horizontal axis shows the azimuthal angle ϕ from 0° to 360°. The vertical axis shows the zenith angle θ from 0° to 180°. The color bar shows the range of realized gain in dB.

elements, and N_e is the number of elements, as shown in Fig. 4. β_i varies from $-5\pi/6$ to $5\pi/6$ for every $\pi/6$. For the patch array, the scan angle of the ith beam in the azimuthal plane can be approximately found by [27]

$$\phi_{\mathrm{m},i} = \cos^{-1}\left(\frac{\lambda_0 \beta_i}{2\pi D}\right) + \frac{\pi}{2}. \qquad (3)$$

The scan angles of other arrays can be approximately found in a similar manner. (3) is also used below to calculate the progressive phase shift angle β_i for arrays with greater element spacing D but the same scan angles. The total input power[3] is set to $P_{\mathrm{in}} = 20$ dBm, which is lower than the maximum transmit power of 4G UE (23 dBm) [28] and the 3GPP requirements on the maximum TRP at 28 GHz (see Table 1).

The fields simulated in the commercial full-wave simulation software CST MWS were saved on a regular grid with a sampling width of 1 mm on planes parallel to the UE surfaces. These data were post-processed to calculate incident power density. The incident power density was averaged over the square-shape area for those planes perpendicular to the UE surfaces.
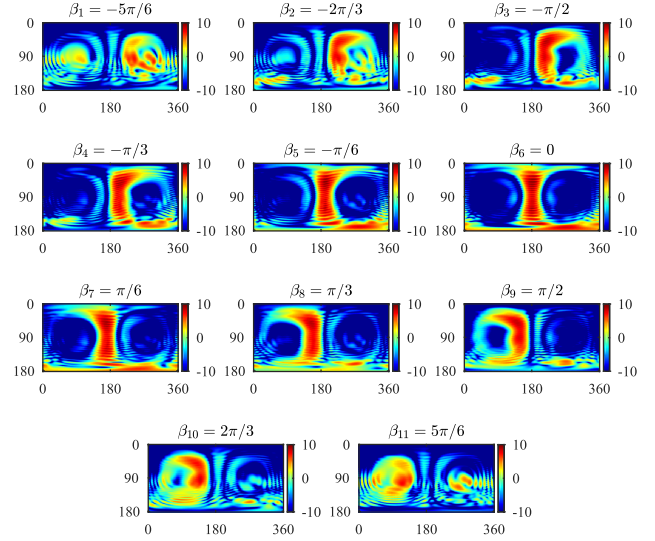
B. RADIATION PERFORMANCE

Fig. 5 shows the scan patterns of the 4 × 1 patch array with $D = 5$ mm. The asymmetry of the scan patterns can be attributed to the asymmetry of the mock-up. Using the same code book, the notch array and the slot array have similar scan capabilities. Fig. 6 shows the total scan patterns of these arrays. The patch array and the notch array are more directive, while the slot array is more omnidirectional. Ripples can be observed in their total scan patterns due to the effects of the realistic housing integration [29], [30]. The maximum realized gain $G_{\mathrm{r,max}} = \max\limits_{i=1,2,\ldots,N_b} G_r(\mathbf{w}_i)$ is about 10 dBi for all three arrays, where $G_r(\mathbf{w}_i)$ denotes the realized gain of the ith beam.
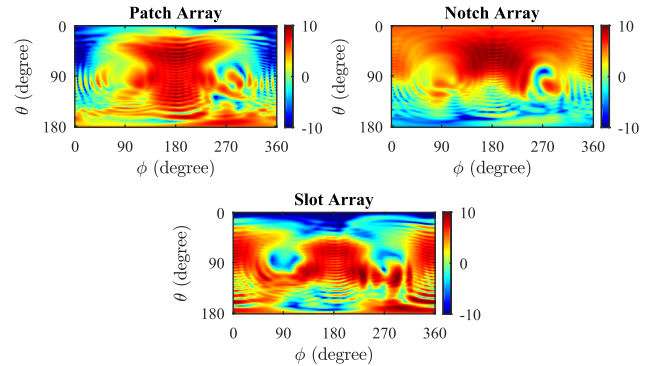
C. MAXIMUM INCIDENT POWER DENSITY LIMIT AND ITS RESTRICTION ON PEAK EIRP

Fig. 7 shows the results of (1) for different phase shift angles β_i and different separation distances d. For beamforming

[3]Here the input power is defined as $P_{\mathrm{in}} = \mathrm{TRP}/[e_r(1 - |\Gamma|^2)]$, where e_r is the radiation efficiency, and Γ is the reflection coefficient.

FIGURE 6. Total scan patterns of the 28 GHz mock-ups containing 4 × 1 arrays ($D = 5$ mm). The color bar shows the range of realized gain in dB.

arrays, the maximum gain usually occurs in the boresight direction and drops towards the end-fire direction. The variation of $S(d, \mathbf{w}_i)$ against β_i for large d is approximately in accordance with the variation of gain, but this does not hold true in the proximity of the UE. A similar phenomenon was reported in [19] for the spatial-peak incident power density. This could be attributable to the pattern enhancement due to the surface currents along the chassis when the beam is steered to large scan angles, suggesting that all possible excitations should be tested to state compliance.

Based on (1) and (2), the maximum allowed input power to be compliant with the incident power density limits S_{lim} can be written as

$$P_{\mathrm{in,max}} = \max_{d \geq d_s} \frac{S_{\mathrm{lim}} P_{\mathrm{in}}}{S_{\mathrm{max}}(d)}, \qquad (4)$$

in which d_s is the test separation distance. At and above the test separation distance, incident power density must be
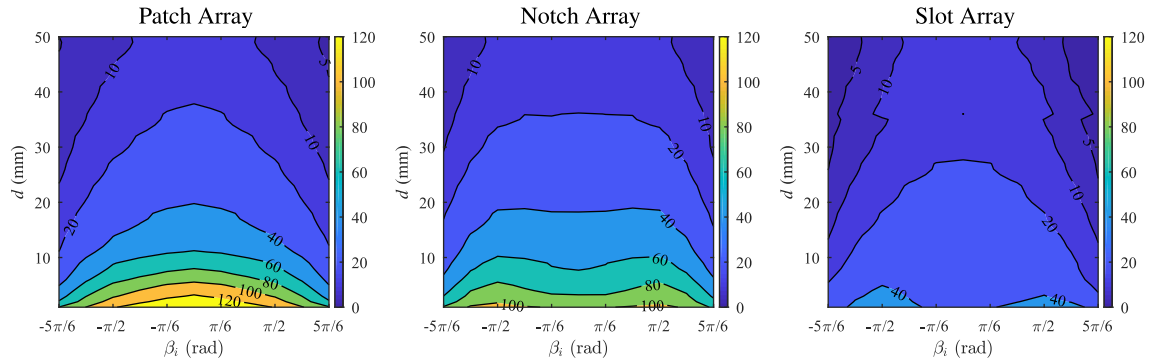
FIGURE 7. Maximum $4\,\text{cm}^2$-averaged incident power density when d and β_i vary for 28 GHz 4×1 arrays ($D = 5\,\text{mm}$, $P_{\text{in}} = 20\,\text{dBm}$). The color bars show the incident power density ranges in W/m^2.

TABLE 3. The maximum allowed input power and EIRP to be compliant with the proposed incident power density limits for 28 GHz 4×1 arrays ($D = 5\,\text{mm}$).

| Element Type	$P_{\text{in,max}}$ (dBm)	EIRP_{max} (dBm)
Proposed ICNIRP/IEEE limits		
Patch	14.6	24.6
Notch	15.6	25.6
Slot	18.8	29.2
Proposed FCC Limits		
Patch	9.7	19.8
Notch	10.8	20.7
Slot	14.0	24.4

below the limit. In this paper, $d_s = 5\,\text{mm}$ [31] is selected to be consistent with the European Committee for Electrotechnical Standardization (CENELEC) standard EN 50566 [32], in which a test separation distance of 5 mm or less should be used for compliance assessments of body worn, body supported or garment integrated devices when measuring SAR. The FCC currently specifies $d_s = 50\,\text{mm}$ for incident power density measurements but has noticed that such a large distance does not make sense in the context of 5G UE working closely to human bodies and has proposed to change [33]. Using (4), the maximum allowed peak EIRP in dB can be expressed as

$$\text{EIRP}_{\text{max}} = P_{\text{in,max}} + G_{\text{r,max}}. \qquad (5)$$

Table 3 presents $P_{\text{in,max}}$ and the corresponding EIRP_{max} to be compliant with the proposed ICNIRP, IEEE, and FCC incident power density limits. Below 30 GHz, the proposed ICNIRP limits and the proposed IEEE limits have the same limit values and the same averaging area (see Table 2). With similar array structure and housing conditions, the bi-directional slot array is allowed to have the highest $P_{\text{in,max}}$ and EIRP_{max}, as the radiated power is distributed on both sides of the chassis. The notch element and the patch element are the uni-directional type, while the patch element has narrower beamwidth than the notch element, and the patch array has less solid angle coverage than the notch array. This might be the reason that the patch array has the lowest $P_{\text{in,max}}$ and EIRP_{max}. Generally, the proposed ICNIRP and IEEE
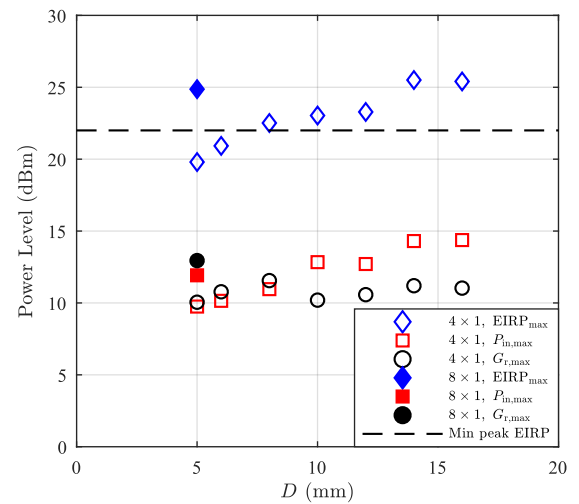
FIGURE 8. The maximum allowed input power $P_{\text{in,max}}$, the maximum realized gain $G_{\text{r,max}}$, and resulting maximum allowed peak EIRP EIRP_{max} for 28 GHz mock-ups containing 4×1 and 8×1 patch arrays to be compliant with the proposed FCC limits. The dashed line is the 3GPP requirement on the minimum peak EIRP (i.e., 22.4 dBm).

limits have extra 5 dB margin in EIRP_{max} compared to the proposed FCC limits at 28 GHz.

D. PARAMETRIC STUDY: INCREASED ELEMENT SPACING AND NUMBER OF ELEMENTS

As the patch array configuration is allowed to transmit with a relatively lower EIRP_{max} among the investigated mock-ups, the following analysis, including the 28 GHz parametric study in this section and the 39 GHz study in the next section, is exemplified by the patch array.

Fig. 8 shows the results of the parametric analysis of the 4×1 patch array by increasing the element spacing D from 5 mm up to 16 mm. From $D = 5\,\text{mm}$ to 8 mm, more power is allowed to be transmitted, as the radiated power is less localized. Above $D = 8\,\text{mm}$, the general trend is still that more power can be allowed to transmit as D increases, but when D^2 is close to the size of the averaging area, some fluctuation in $P_{\text{in,max}}$ can be observed. When $D < 10\,\text{mm}$,

TABLE 4. The maximum EIRP to be compliant with the proposed incident power density limits for the 39 GHz patch arrays.

Number of Elements N_e	$\mathrm{EIRP_{max}}$ (dBm)
Proposed ICNIRP limits	
4×1	23.0
8×1	27.2
Proposed IEEE Limits	
4×1	25.9
8×1	28.9
Proposed FCC Limits	
4×1	21.3
8×1	24.3
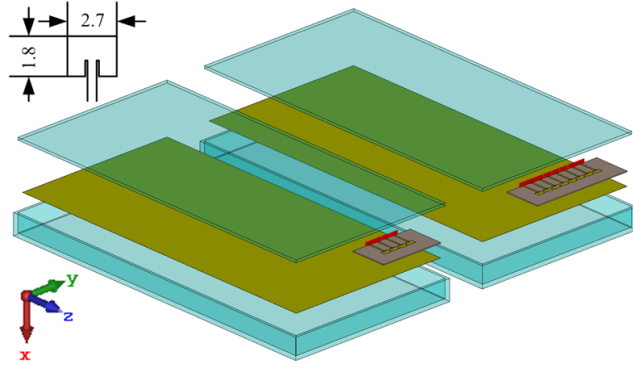
FIGURE 9. Exploded view of simulation models of 39 GHz UE mock-ups containing 4×1 (left) and 8×1 (right) patch arrays ($D = 3.6$ mm). The inset shows the dimension of the element.

$G_{r,max}$ increases with D. The sudden drop in $G_{r,max}$ at $D = 10$ mm is due to the inevitable excitation of grating lobes,[4] though the grating lobe can still be excited for large scan angles when $\lambda_0/2 < D < \lambda_0$. In Fig. 8, the results of the 8×1 patch array with $D = 5$ mm are also plotted, which provide a great margin in $\mathrm{EIRP_{max}}$.

IV. RF EMF EXPOSURE LIMIT IMPACTS ON PEAK EIRP AT 39 GHz

A. SIMULATION SETTINGS

Fig. 9 shows the simulation models of UE mock-ups operating at 39 GHz. One contains a 4×1 patch array, and the other contains an 8×1 patch array with the identical element dimension and element spacing $D = 3.6$ mm ($0.47\lambda_0$ at 39 GHz, same as $D = 5$ mm at 28 GHz). The other simulation settings and post-processing procedures are identical as in the previous section.

B. IMPACTS ON PEAK EIRP

Above 30 GHz, the proposed ICNIRP limits and the proposed IEEE limits are averaged over 1 cm^2 and 4 cm^2, respectively (see Table 2). By repeating the analysis procedures in the previous section, Table 4 shows the maximum EIRP to be compliant with the proposed incident power density limits.

---

[4]Although $D = 10$ mm is slightly shorter than λ_0 at 28 GHz, very strong side lobes in the end-fire directions can be observed even for the boresight beam due to the realistic housing integration. Such kind of side lobes could also be seen as the grating lobes.

The 4×1 patch array, even with the element spacing of approximately half wavelength, can meet the 3GPP requirements on the minimum peak EIRP in the 39 GHz band (see Table 1).

C. IMPACTS OF HOUSING ENVIRONMENTS

In [20], ideal ground-backed dipole arrays were used to calculate the maximum allowed transmit power and maximum allowed EIRP, the conclusion of which is that the maximum allowed EIRP would drop as the frequency increases for the same element spacing in terms of free space wavelength and the same number of antenna elements. However, in this paper, Table 3 and Table 4 show the opposite, i.e., $\mathrm{EIRP_{max}}$ for the proposed IEEE and FCC limits is higher at the higher frequency. This can be attributed to the realistic housing integration. $\mathrm{EIRP_{max}}$ for the proposed ICNIRP limits are not comparable due to the change of the size of the averaging area.

The radiation performance of the integrated mmWave antennas suffers from the housing environments, more severe than today's UE operating below 6 GHz. To evaluate how housing integration affects the coverage performance, the effective beam-scanning efficiency is proposed in [30], which is expressed as

$$\eta_{\mathrm{EBS}}\left(G_{r,th}, \Omega_d\right) = \frac{\int_{\Omega_d} |F_{\mathrm{TS}}(\Omega)|^2 \, h\left(G_{r,\mathrm{TS}}(\Omega)\right) d\Omega}{\int_{\Omega_0} |F_{\mathrm{TS}}(\Omega)|^2 \, d\Omega}, \quad (6)$$

in which $G_{r,th}$ is the threshold realized gain to establish the radio access, Ω_d is the spherical coverage in solid angles without the effects of housing integration, i.e., desired spherical coverage, $\Omega_0 = 4\pi$ is the full spherical solid angles, $G_{r,\mathrm{TS}}$ denotes the total scan pattern, and $|F_{\mathrm{TS}}(\Omega)|$ denotes the far-field strength of the total scan pattern, and h is a step function

$$h\left(G_{r,\mathrm{TS}}\right) = \begin{cases} 1 & G_{r,\mathrm{TS}} \geq G_{r,th} \\ 0 & G_{r,\mathrm{TS}} < G_{r,th}. \end{cases} \quad (7)$$

If a beamforming array is less affected by housing integration, it leads to less distorted coverage and a high η_{EBS}. In contrast, the severely-distorted coverage gives a low η_{EBS}. As the 28 GHz patch array in the previous section and the 39 GHz patch array in this section are provided with the same housing integration, the same code book, and the same element spacing in terms of free space wavelength, their η_{EBS} for $\Omega_d = \{\theta \in [15°, 165°], \phi = [105°, 255°]\}$ shown in Fig. 10 is comparable for the effects of housing integration. The η_{EBS} of the 28 GHz array is generally higher than the η_{EBS} of the 39 GHz array, indicating that the housing integration has greater impact on the 39 GHz array. More power is radiated through chassis and casing. This results in the lower exposure, higher allowed transmit power, and higher EIRP. The detailed analysis about how the radiated power is guided towards unwanted directions in 5G UE can be found in [30].
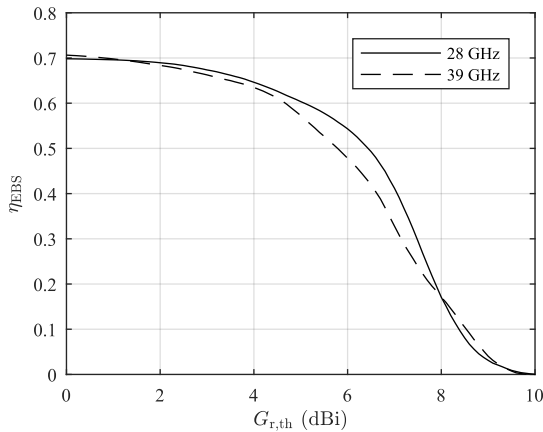
FIGURE 10. The effective beam-scanning efficiency η_{EBS} for the 28 GHz 4 × 1 patch array with $D = 5$ mm and 39 GHz 4 × 1 patch array with $D = 3.5$ mm.

(a)

(b)
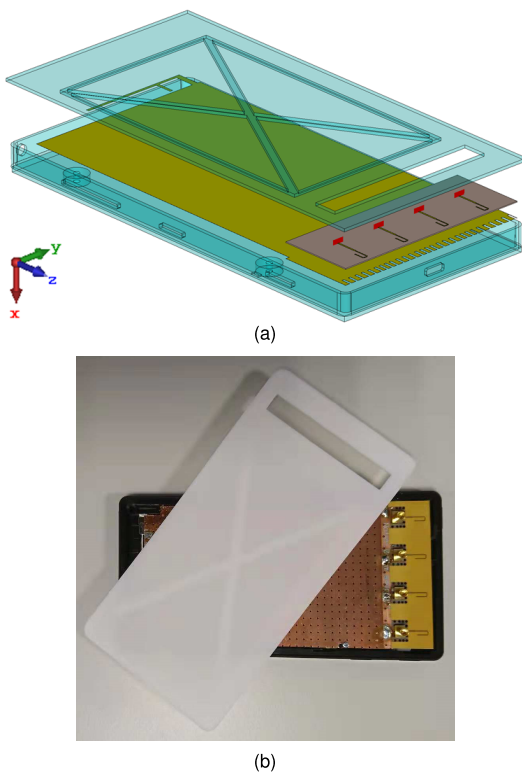
FIGURE 11. 28 GHz UE mock-up containing a 4 × 1 notch array provided for IEC TR 63170 [34]. (a) exploded view of the simulation model (b) mock-up fabricated by Sony Mobile.

V. DISCUSSION

Fig. 11 shows a 28 GHz UE mock-up containing a 4 × 1 notch array, which is designed by one of the authors of this paper and fabricated by Sony Mobile, provided to the International Electrotechnical Commission (IEC) Technical Committee (TC) 106. From 2017 to 2018, TC 106 developed the technical report IEC TR 63170 [34] specifying the state-of-the-art of measurement techniques and test approaches for evaluating portable devices based on incident power density measurements from 6 GHz to 100 GHz. In Annex H

of [34], the results of measured incident power conducted on the provided UE mock-up are presented. Three laboratories applied different systems and techniques to assess incident power density in close proximity of the mock-up. One laboratory measured the amplitude of the electric field components. In case the phases of the electric and/or magnetic fields cannot be measured directly, they can be numerically retrieved from multiple measurements of the field amplitudes [35]. One laboratory measured both amplitude and phase of the electric fields on the measurement surface and reconstructed the electric and magnetic fields on the evaluation plane based on the solution of an inverse source problem [36]. Another laboratory applied a two-probe method where both electric and magnetic field components are measured. This technique does not make use of reconstruction algorithm as both electric and magnetic fields are directly measured on the evaluation surface [37]. The measurement results from the three laboratories using different systems and techniques agree well with each other, as well as with the simulation results. The detailed description about the mock-up configuration, measurement set-ups, procedures, and results can be found in [34].

The previous studies on output power levels of mmWave UE [18]–[20] suggest that it might be difficult to allow a single element or small arrays transmitting enough power considering the current incident power density limits. The findings in this paper show that the 3GPP requirements on the minimum peak EIRP for UE can generally be satisfied when considering the RF EMF exposure restrictions in the 28 GHz and 39 GHz bands, in line with the main conclusion drawn in [38] and [39]. The antenna configuration and integration are likely to play a large role in determining compliance with the RF EMF exposure limits. The RF EMF exposure generated by realistic UE containing other components can be expected even lower due to much more deteriorated radiation [30]. In addition, as the RF EMF exposure limits are intended to be averaged over time, for time division duplex (TDD) systems, the transmit power and EIRP during uplink transmission should be scaled up according to the applicable duty cycle (e.g., +6 dB for a downlink-to-uplink duty cycle ratio of 75% : 25% compared with the results presented in this paper).

As for TRP, this paper shows a large margin for 4- and 8-element arrays operating at 28 GHz and 39 GHz bands to reach the 3GPP requirements on the maximum allowed TRP. Another 3GPP requirements is the EIRP at 50th percentile of Cumulative Distribution Function (CDF) (see Table 1). The CDF results of the mock-up containing patch arrays are shown in Appendix, which shows that the 50th percentile of CDF can meet the corresponding requirements as long as the peak EIRP fulfills the requirements. However, we cannot draw a generic conclusion on that because the EIRP at 50th percentile of CDF is more determined by the code book. Though not rigorous, such results provide an intuitive insight on that.

Increasing element spacing can effectively create greater margin on EIRP. According to the antenna array theory [27],
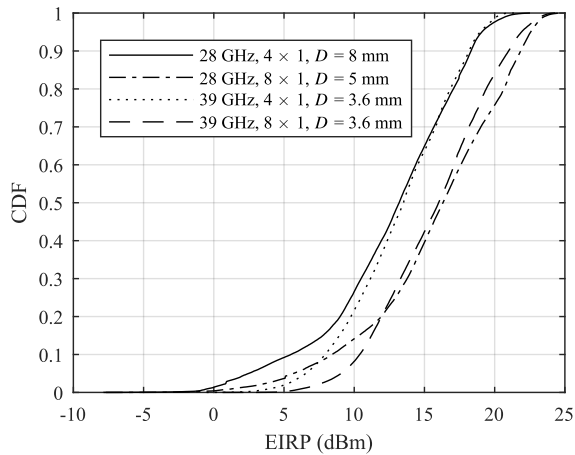
FIGURE 12. CDF of maximum allowed EIRP to be compliant with the proposed FCC incident power density limits for total scan pattern of mock-up using patch arrays.

when the element spacing is greater than half a wavelength but smaller than one wavelength, grating lobes will appear for large scan angles. When the element spacing is greater than one wavelength, grating lobes are inevitable. However, due to the NR beam-centric principle, a grating lobe generated by one UE has less chance to align with the receive beams of another UE or base station. Even if they are aligned, as the peak EIRP levels of 5G beamforming UE are similar to the maximum transmit power levels of 4G UE (23 dBm) [28], the interference levels caused by grating lobes may be similar to interference caused by the 4G UE. Thus, increasing element spacing might be a possible solution even on the system level. However, this needs extensive studies beyond the scope of this paper.

Compared with the 4×1 array configuration, the 8×1 configuration shows a tremendous advantage in performance. Not only can a large margin for meeting both requirements be obtained, but also extra beamforming gain. However, the extra number of elements requires more space for antennas and more complicated RF design.

Section III indicates that the slot array is allowed to achieve higher peak EIRP due to the bi-directional radiation, however, [30] shows that the beamforming performance of the slot array might be deteriorated in a more realistic housing integration when including the display and other components, such as cameras, batteries, etc. Therefore, there is no generic conclusion that the slot is a better option than other types of elements.

VI. CONCLUSION

We have investigated the maximum EIRP that can be achieved for 28 GHz and 39 GHz beamforming UE under the constraints of the proposed incident power density limits. Various types of antenna elements, as well as different sizes of linear arrays and element spacing, have been examined. The typical maximum EIRP values have been given in the paper. The results have shown that the 3GPP 5G NR specification (Release 15) of the minimum peak EIRP for UE can be

generally met when complying with the proposed ICNIRP, IEEE, and FCC exposure limits.

APPENDIX
EIRP AT 50th PERCENTILE OF CDF

Fig. 12 shows the CDF of EIRP of the total scan pattern for the 28 GHz and 39 GHz patch arrays complying with the proposed FCC limits. $D = 8\,\text{mm}$ was chosen for the 28 GHz 4×1 patch array, as its peak EIRP is higher than 22.4 dBm (see Fig. 8). The EIRP at the 50th percentile of CDF is 13.2 dBm, 13.5 dBm, 16.0 dBm, and 16.3 dBm for the CDFs presented in Fig. 12, all above the 3GPP requirements (see Table 1).

REFERENCES
[1] *Final Acts WRC-15 World Radiocommunication Conference*, ITU-R, Geneva, Switzerland, 2015.
[2] *User Equipment (UE) Radio Transmission and Reception. Part 2: Range 2 Standalone*, document TS 38.101-2, 3GPP, Rev. 15.3.0, Sep. 2018.
[3] W. Hong, K.-H. Baek, Y. Lee, Y. Kim, and S.-T. Ko, "Study and prototyping of practically large-scale mmWave antenna systems for 5G cellular devices," *IEEE Commun. Mag.*, vol. 52, no. 9, pp. 63–69, Sep. 2014.
[4] J. Helander, K. Zhao, Z. Ying, and D. Sjöberg, "Performance analysis of millimeter-wave phased array antennas in cellular handsets," *IEEE Antennas Wireless Propag. Lett.*, vol. 15, pp. 504–507, 2016.
[5] Y.-W. Hsu, T.-C. Huang, H.-S. Lin, and Y.-C. Lin, "Dual-polarized quasi Yagi–Uda antennas with endfire radiation for millimeter-wave MIMO terminals," *IEEE Trans. Antennas Propag.*, vol. 65, no. 12, pp. 6282–6289, Dec. 2017.
[6] N. Ojaroudiparchin, M. Shen, S. Zhang, and G. F. Pedersen, "A switchable 3-D-coverage-phased array antenna package for 5G mobile terminals," *IEEE Antennas Wireless Propag. Lett.*, vol. 15, pp. 1747–1750, 2016.
[7] S. Zhang, X. Chen, I. Syrytsin, and G. F. Pedersen, "A planar switchable 3-D-coverage phased array antenna and its user effects for 28-GHz mobile terminal applications," *IEEE Trans. Antennas Propag.*, vol. 65, no. 12, pp. 6413–6421, Dec. 2017.
[8] B. Yu, K. Yang, C.-Y.-D. Sim, and G. Yang, "A novel 28 GHz beam steering array for 5G mobile device with metallic casing application," *IEEE Trans. Antennas Propag.*, vol. 66, no. 1, pp. 462–466, Jan. 2018.
[9] I. Syrytsin, S. Zhang, G. F. Pedersen, and A. S. Morris, "Compact quad-mode planar phased array with wideband for 5G mobile terminals," *IEEE Trans. Antennas Propag.*, vol. 66, no. 9, pp. 4648–4657, Sep. 2018.
[10] *Radiofrequency Radiation Exposure Limits*, FCC, Washington, DC, USA, 2013.
[11] Technical Analysis Branch, Office of Engineering and Technology, FCC. (Oct. 2018). *RF Exposure: Order/NPRM Issues..* [Online]. Available: https://transition.fcc.gov/oet/ea/presentations/files/oct18/5.1-TCB-RF-Exposure-OrderNPRM-Issues-MD.PDF
[12] ICNIRP, "Guidelines for limiting exposure to time-varying electric, magnetic, and electromagnetic fields (up to 300 GHz)," *Health Phys.*, vol. 74, no. 4, pp. 494–522, Apr. 1998.
[13] *Draft Guidelines for Limiting Exposure to Time-Varying Electric, Magnetic and Electromagnetic Fields (100 kHz to 300 GHz)*, document, ICNIRP, Jul. 2018.
[14] *IEEE Standard for Safety Levels With Respect to Human Exposure to Radio Frequency Electromagnetic Fields, 3 kHz to 300 GHz*, IEEE Standard C95.1-2005, 2006.
[15] *IEEE Standard for Safety Levels With Respect to Human Exposure to Radio Frequency Electromagnetic Fields, 3 kHz to 300 GHz Amendment 1: Specifies Ceiling Limits for Induced and Contact Current, Clarifies Distinctions Between Localized Exposure and Spatial Peak Power Density*, IEEE Standard C95.1a-2010, 2010.

[16] *IEEE Draft Standard for Safety Levels With Respect to Human Exposure to Electric, Magnetic and Electromagnetic Fields, 0 Hz to 300 GHz*, IEEE Draft Standard PC95.1/D3.5, Oct. 2018.

[17] *Notice of Proposed Rulemaking*, FCC, Washington, DC, USA, 2015, pp. 15–138.

[18] D. Colombi, B. Thors, and C. Törnevik, "Implications of EMF exposure limits on output power levels for 5G devices above 6 GHz," *IEEE Antennas Wireless Propag. Lett.*, vol. 14, pp. 1247–1249, 2015.

[19] K. Zhao, Z. Ying, and S. He, "EMF exposure study concerning mmWave phased array in mobile devices for 5G communication," *IEEE Antennas Wireless Propag. Lett.*, vol. 15, pp. 1132–1135, 2016.

[20] B. Thors, D. Colombi, Z. Ying, T. Bolin, and C. Törnevik, "Exposure to RF EMF from array antennas in 5G mobile communication equipment," *IEEE Access*, vol. 4, pp. 7469–7478, 2016.

[21] K. Foster and D. Colombi, "Thermal response of tissue to RF exposure from canonical dipoles at frequencies for future mobile communication systems," *Electron. Lett.*, vol. 53, no. 5, pp. 360–362, Mar. 2017.

[22] B. Xu *et al.*, "Power density measurements at 15 GHz for RF EMF compliance assessments of 5G user equipment," *IEEE Trans. Antennas Propag.*, vol. 65, no. 12, pp. 6584–6595, Dec. 2017.

[23] W. He, B. Xu, M. Gustafsson, Z. Ying, and S. He, "RF compliance study of temperature elevation in human head model around 28 GHz for 5G user equipment application: Simulation analysis," *IEEE Access*, vol. 6, pp. 830–838, 2018.

[24] *Draft Guidelines for Limiting Exposure to Time-Varying Electric, Magnetic and Electromagnetic Fields (100 kHz to 300 GHz). Appendix A: Review of Studies on Dosimetry*, document, ICNIRP, Jul. 2018.

[25] *Draft Guidelines for Limiting Exposure to Time-Varying Electric, Magnetic and Electromagnetic Fields (100 kHz to 300 GHz). Appendix B: Health Risk Assessment Literature*, document, ICNIRP, Jul. 2018.

[26] B. Xu, M. Gustafsson, S. Shi, K. Zhao, Z. Ying, and S. He, "Radio frequency exposure compliance of multiple antennas for cellular equipment based on semidefinite relaxation," *IEEE Trans. Electromagn. Compat.*, vol. 61, no. 2, pp. 327–336, Apr. 2019.

[27] C. A. Balanis, *Antenna Theory: Analysis and Design*, 4th ed. Hoboken, NJ, USA: Wiley, 2016, ch. 5, pp. 285–384.

[28] *User Equipment (UE) Radio Transmission and Reception*, document TS 36.101, 3GPP, Rev. 14.9.0, 2018.

[29] B. Xu, K. Zhao, Z. Ying, S. He, and J. Hu, "Investigation of surface waves suppression on 5G handset devices at 15 GHz," in *Proc. 10th Eur. Conf. Antennas Propag. (EuCAP)*, Apr. 2016, pp. 1–4.

[30] B. Xu *et al.*, "Radiation performance analysis of 28 GHz antennas integrated in 5G mobile terminal housing," *IEEE Access*, vol. 6, pp. 48088–48101, 2018.

[31] D. Colombi, B. Thors, C. Törnevik, and Q. Balzano, "RF energy absorption by biological tissues in close proximity to millimeter-wave 5G wireless equipment," *IEEE Access*, vol. 6, pp. 4974–4981, 2018.

[32] *Product Standard to Demonstrate the Compliance of Wireless Communication Devices With the Basic Restrictions and Exposure Limit Values Related to Human Exposure to Electromagnetic Fields in the Frequency Range From 30 MHz to 6 GHz: Hand-Held and Body Mounted Devices in Close Proximity to the Human Body*, CENELEC Standard EN 50566, Oct. 2017.

[33] *First Report and Order, Further Notice of Proposed Rule Making, and Notice of Inquiry*, FCC, Washington, DC, USA, 2013, pp. 13–39.

[34] *Measurement Procedure for the Evaluation of Power Density Related to Human Exposure to Radio Frequency Fields From Wireless Communication Devices Operating Between 6 GHz and 100 GHz*, document TR 63170, IEC, Aug. 2018.

[35] S. Pfeifer *et al.*, "Total field reconstruction in the near field using pseudo-vector *E*-field measurements," *IEEE Trans. Electromagn. Compat.*, vol. 61, no. 2, pp. 476–486, Apr. 2019.

[36] J. Lundgren, J. Helander, M. Gustafsson, D. Sjöberg, B. Xu, and D. Colombi, "Near-field measurement and calibration technique for compliance testing of mm-wave 5G devices," *Sci. Rep.*, to be published.

[37] M. Nesterova, S. Nicol, and Y. Nesterova, "Evaluating power density for 5G applications," in *Proc. IEEE 5G World Forum (5GWF)*, Jul. 2018, pp. 347–350.

[38] *Uplink Duty Cycle and Power Back-Off Considerations for FR2*, document R4-1813526, 3GPP, Aug. 2018.

[39] *Update on RF EMF Regulations of Relevance for Handheld Devices Operating in the FR2 Bands*, document R4-1814719, 3GPP, Nov. 2018.

BO XU (S'14–M'18) received the B.E. degree in information engineering and the Ph.D. degree in optical engineering from Zhejiang University, Hangzhou, Zhejiang, China, in 2010 and 2017, respectively. He is in a joint Ph.D. program between the Department of Electromagnetic Engineering, KTH Royal Institute of Technology, Stockholm, Sweden, and the Centre for Optical and Electromagnetic Research, Zhejiang University. He was a Visiting Student with the Department of Electrical and Information Technology, Lund University, Lund, Sweden, in 2016 and 2017.

Since 2018, he has been an Experienced Researcher with Ericsson Research, Ericsson AB, Stockholm. His research interests include EMF health and safety, antenna design and measurement, and RFID.

KUN ZHAO received the B.S. degree in communication engineering from the Beijing University of Posts and Telecommunications, Beijing, China, in 2010, the M.S. and Ph.D. degrees from the Royal Institute of Technology (KTH), Stockholm, Sweden, in 2012 and 2017, respectively.

He is currently a Researcher of antenna technology and standardization with the Department of Research and Standardization, Sony Mobile Communication AB, Lund, Sweden. Frequently a 3GPP RAN 4 delegate. He is also an Industrial Postdoctoral in antennas, propagation, and radio networking with Aalborg University, Aalborg, Denmark. He has been a Visiting Researcher with the Department of Electrical and Information Technology, Lund University, Sweden. His current research interests include mm-wave antenna and propagation for 5G communications, MIMO antenna systems, user body interactions, and body centric wireless communications.

ZHINONG YING (SM'05) received the M.Sc. degree in electrical engineering from the Beijing University of Posts and Telecommunications, Beijing, China, in 1986, and the Licentiate degree in microwave engineering from the Chalmers University of Technology, Gothenburg, Sweden, in 1995.
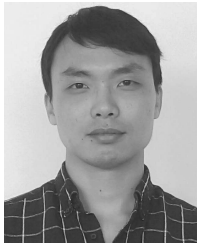
He joined Ericsson AB, in 1995. He became a Senior Specialist, in 1997, and an Expert, in 2003, in his engineer career with Ericsson. He has also been a Guest Professor with the Joint Research Centre, Royal Institute of Technology, Sweden, and Zhejiang University, China, since 2001. He is currently a Principal Engineer of antenna technology with the Network Technology Lab, Research and Technology, Sony Mobile Communications AB, Lund, Sweden, and also as a Distinguish Engineer, Sony Group. He has authored and co-authored over 140 papers in various journal, conference, and industry publications. He holds more than 147 patents and pending in the antennas and new generation wireless network areas. He contributed several book chapters on mobile antenna, small antenna, and MIMO antennas in *Mobile Antenna Handbook* Third Edition (H. Fujimoto) and *Handbook of Antenna Technologies* (Z. N. Chen). He had contributed a lot of work in antenna designs and evaluation methods for the mobile industry. He has also involved in the evaluation of Bluetooth technology which was invented by Ericsson. His main research interests are small antennas, broad- and multi-band antenna, multi-channel antenna (MIMO) systems, antenna for body area networks, antenna and propagation in fifth generation mobile networks, including massive MIMO and mmWave, and near-field and human body effects and measurement techniques.

Dr. Ying was a member of the Scientific Board of the ACE Program (Antenna Centre of Excellent in European 6th frame), from 2004 to 2007. He is a Senior Member of the IEEE. He served as a TPC Co-Chairman of the International Symposium on Antenna Technology (iWAT), 2007, and served as a Session Organizer of several international conferences, including IEEE APS, and a Reviewer for several academic journals. He received the Best Invention Award from Ericsson Mobile, in 1996, and the Key Performer Award from Sony Ericsson, in 2002. He was nominated for the President Award by Sony Ericsson, in 2004, for his innovative contributions. He received the Distinguish Engineer title by Sony Group globally, in 2013.

DANIEL SJÖBERG (M'11–SM'17) received the M.Sc. degree in engineering physics and the Ph.D. degree in engineering, electromagnetic theory from Lund University, Lund, Sweden, in 1996 and 2001, respectively. In 2001, he joined the Electromagnetic Theory Group, Lund University, where, in 2005, he became a Docent in electromagnetic theory, where he is currently a Professor and the Head of the Department of Electrical and Information Technology. His research interests include the electromagnetic properties of materials, composite materials, homogenization, periodic structures, numerical methods, radar cross section, wave propagation in complex and nonlinear media, and inverse scattering problems.

SAILING HE (M'92–SM'98–F'13) received the Licentiate and Ph.D. degrees in electromagnetic theory from the KTH Royal Institute of Technology, Stockholm, Sweden, in 1991 and 1992, respectively, where he has been with the Department of Electromagnetic Theory, as an Assistant Professor, an Associate Professor, and a Full Professor, since 1992. He also serves as the Director for a joint research center between KTH and Zhejiang University, China. He has first-authored one monograph (Oxford University Press) and authored/co-authored about 500 papers in refereed international journals. He has given many invited/plenary talks in international conferences, and has served in the leadership for many international conferences. His current research interests include applied electromagnetics, electromagnetic metamaterials, optoelectronics, microwave photonics, and biomedical applications.

● ● ●

WANG HE received the B.E. degree in information engineering from Zhejiang University, Hangzhou, China, in 2015, where he is currently pursuing the Ph.D. degree with the Centre for Optical and Electromagnetic Research. His current research interests include antenna design, RFID technology, and RF EMF exposure.